DOI: 10.1002/anie.200907021

Doped Nanostructures

Diluted Magnetic Semiconductor Nanowires Prepared by the Solution–Liquid–Solid Method**

Zhen Li, Lina Cheng, Qiao Sun, Zhonghua Zhu, Mark J. Riley, Muhsen Aljada, Zhenxiang Cheng, Xiaolin Wang, Graeme R. Hanson, Shizhang Qiao, Sean C. Smith, and Gao Qing (Max) Lu**

In recent years, paramagnetic-ion-doped semiconductor nanostructures (diluted magnetic semiconductors, DMSs) such as dots, rods, wires, and films have been the subject of intense research because of their fascinating properties (for example, the magnetism of doped nanocrystals can be either induced by charge or light) and potential applications in bioimaging, solar cells, spintronics, and quantum interference information processing.[1–12] Traditionally, these DMS nanostructures were generated by expensive non-wet chemical methods such as molecular-beam epitaxy (MBE), vapor–liquid–solid (VLS) and chemical vapor deposition (CVD) techniques.[7,10] The nanostructures thus obtained do not always fall within the quantization regime and exhibit weakly enhanced carrier/paramagnetic ion spin interactions. Additionally, the lack of surface ligands on the nanostructures limits their solubility, surface functionalization, processability, and applications. Thus the preparation of colloidal DMS nanostructures within the quantization regime through a simple wet-chemical approach remains a great challenge.

Recently, there have been extensive reports on the preparation of high-quality DMS nanocrystals,[1–7] nanorods,[8] and nanoribbons[9] by advanced colloidal chemistry, but only few reports on the wet-chemical synthesis of DMS nanowires,[11] despite their unique advantages in fabricating electronic devices compared with dots and rods. Herein, we report the first example of manganese-doped cadmium selenide (Mn-CdSe) nanowires generated by a solution–liquid–solid (SLS)[13–15] technique, which can provide an alternative and potentially low-cost route towards magnetically active quantum wires. Mn-CdSe was chosen as a target because of its unique magnetic and optical properties.[1] Mn^{2+} ions have the highest effective magnetic moment of the first-row transition-metal ions, and the magnetism of doped nanocrystals can be induced by light. Additionally, the photoluminescent properties of Mn-CdSe can be controlled by either the Mn dopants or by CdSe itself, depending on the size of nanostructures.[1]

The doping of Mn^{2+} ions into a CdSe lattice is notoriously problematic because of the intrinsic "self-purification"[16] and reduced surface adsorption of dopants.[2b] Most doped CdSe nanocrystals have been prepared from air-sensitive precursors or complicated single complexes.[1–3] In our studies, we used low-melting-point Bi nanoparticles as nanoreactors for the doping process. These Bi nanoparticles are melted into droplets at high temperature and serve as catalysts for the nucleation and growth of nanowires.[13–15] The phase diagrams (Figure S1 in the Supporting Information) show that both Mn and CdSe have a similar solubility (ca. 3%) in Bi at the same eutectic temperature (265 °C).[17] Thus it is anticipated that Mn can be doped into CdSe and the doping process will be confined within Bi droplets. We used air-stable cadmium oxide (CdO), manganese stearate ($MnSt_2$), and selenium (Se) as precursors. The nanowires were produced after introducing a mixture of Mn and Se precursors and Bi nanoparticles into Cd precursor solution at 250 °C.

Figure 1 a–c shows the TEM images of the resultant nanowires obtained from 0.25, 0.5, and 1.0 mL Mn precursor solution (25 mg mL^{-1}; Table S1, code 1–3, in the Supporting Information). It can be seen that the influence of the Mn precursor solution on the nanowire length is more pronounced than the influence on the diameter (Figure S2 in the

[*] Dr. Z. Li, L. N. Cheng, Dr. S. Z. Qiao, Prof. G. Q. Lu
ARC Centre of Excellence for Functional Nanomaterials
Australian Institute for Bioengineering and Nanotechnology
The University of Queensland
Queensland, QLD 4072 (Australia)
Fax: (+61) 7-3346-3973
E-mail: z.li3@uq.edu.au
maxlu@uq.edu.au
Homepage: http://www.nanomac.uq.edu.au/index.html
Dr. Q. Sun, Prof. S. C. Smith
Australian Institute for Bioengineering and Nanotechnology
Centre for Computational Molecular Science
The University of Queensland (Australia)
Prof. Z. H. Zhu
School of Chemical Engineering
The University of Queensland (Australia)
Dr. M. J. Riley
School of Chemistry and Molecular Biosciences
The University of Queensland (Australia)
Dr. M. Aljada
Australian National Fabrication Facility (QLD node)
The University of Queensland (Australia)
Dr. Z. X. Cheng, Prof. X. L. Wang
Institute for Superconducting and Electronic Materials
The University of Wollongong (Australia)
Prof. G. R. Hanson
Centre for Magnetic Resonance
The University of Queensland (Australia)

[**] Z.L. gratefully acknowledges the award of a Queensland Smart Future Fellowship, a Queensland International Fellowship, a University of Queensland (UQ) Postdoctoral Fellowship, and a UQ Early-Career-Research Grant.

Supporting information for this article is available on the WWW under http://dx.doi.org/10.1002/anie.200907021.

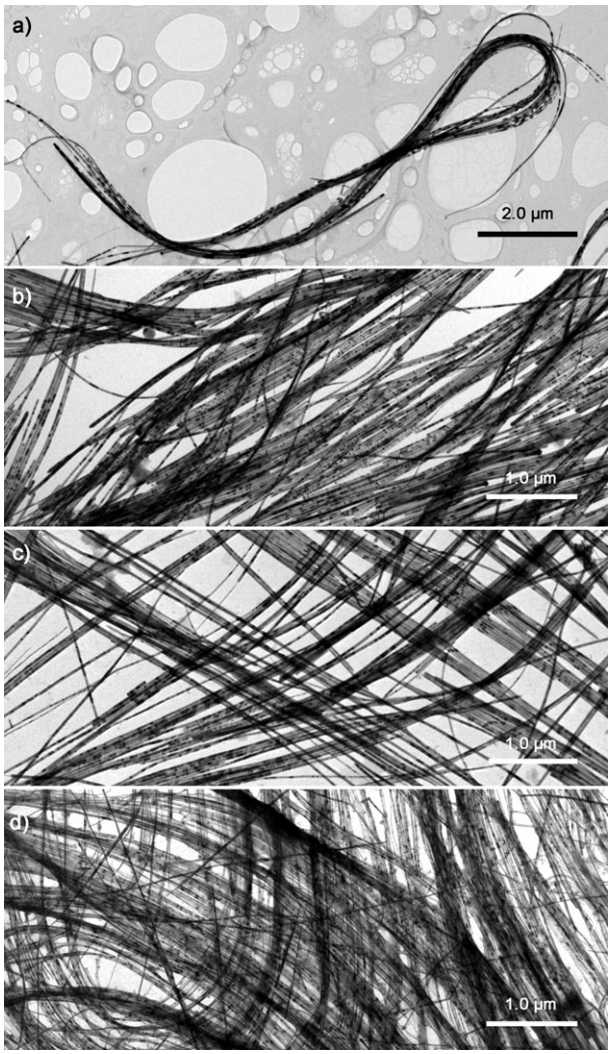

Figure 1. a–c) TEM images of CdSe nanowires doped with 2.1%, 2.6%, and 3.0% Mn. d) TEM image of Mn-doped CdSe nanowires prepared by using double the amounts of Cd and Se precursors.

Supporting Information). When the volume of Mn precursor solution used was increased from 0.25 to 1.0 mL, the nanowire diameter increased from 25.4 to 29.1 nm, but the length notably decreased from tens of micrometers (ca. 15 μm) to several micrometers (ca. 4 μm). It should be noted that the actual Mn content of these three samples was 2.1%, 2.6% and 3.0%, respectively, as determined by inductively coupled plasma mass spectrometry (ICP-MS). These values are lower than those of the injected Mn precursors, that is, 4.7%, 9.0%, and 17.1%, respectively. The lower Mn content might be attributed to several factors such as the low solubility of Mn in Bi (only ca. 3%; Figure S1 in the Supporting Information), the competitively parallel reactions, and the slower decomposition of Mn precursor than the growth of nanowires. For comparison, undoped CdSe nanowires have been prepared under the same conditions in the absence of the Mn precursor (see the Supporting Information, Table S1, code 4). The CdSe nanowires thus obtained have similar diameter ($D = (25.1 \pm 6.4)$ nm, Figure S3 in the Supporting Information) and length to those obtained when 0.25 mL Mn precursor was used.

The broad diameter distribution of the nanowires is attributed to the competition between nanowire growth, Bi nanocatalyst growth, and other processes.[15] The introduction of the Mn precursor depressed the growth of nanowires, and led to thick short nanowires. The strategy for the production of thin long nanowires is to accelerate the growth of nanowires and depress other side reactions by simultaneously controlling several reaction parameters such as concentrations, precursors, stabilizers, and temperatures. Figure 1d shows the TEM image of nanowires obtained by using double the amounts of Cd and TOPSe precursors (Table S1, code 5, in the Supporting Information). These noodle-shaped nanowires are 12.9 nm in diameter and tens of micrometers in length (see Figure S2 in the Supporting Information). Some of the nanowires are below the bulk exciton dimension of CdSe (i.e., 11.2 nm).

Figure 2a,b shows the typical high-resolution TEM images of the thicker and thinner doped nanowires. The clear twinned lattice boundary is due to the fast nanowire

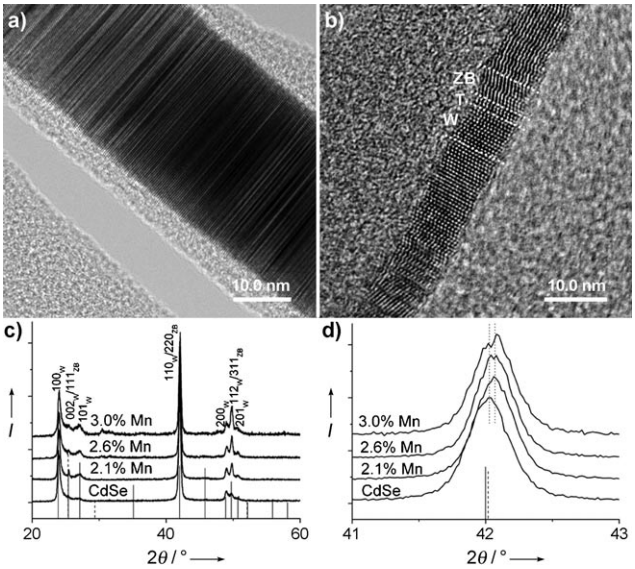

Figure 2. a, b) Typical HRTEM images of thick and thin Mn-doped CdSe nanowires, T denotes a boundary between two ZB segments of different orientation; c, d) XRD patterns of Mn-doped and undoped CdSe nanowires. Stick patterns of wurtzite (solid) and zinc blende (dashed) phases are provided for comparison.

growth and the small energy difference between zinc blende (ZB) and wurtzite (W) structures. This difference leads to an admixture of ZB and W phases, which can be easily seen in the thinner nanowires (Figure 2b).[14] The *d* spacing in the HRTEM images is reduced compared to the standard *d* value of bulk CdSe (Figure S4 in the Supporting Information). The spacing shrinkage is also proved by powder X-ray diffraction (XRD) patterns (Figure 2c) of the as-synthesized nanowires (shown in Figure 1a–c and Figure S3 in the Supporting Information). Both doped and undoped nanowires exhibit a suppression in the $(100)_W$, $(002)_W$, $(101)_W$, and $(111)_{ZB}$ facets,

and an enhancement in the $(110)_W$ and $(220)_{ZB}$ facets compared to bulk W- and ZB-CdSe. Such effects are likely caused by substrate-induced nanowire orientation[14] and the fact that doping and associated defects will occur preferentially on the more highly reactive and faster-growing (001) facets rather than on the less reactive (110) facets. This latter observation is supported by slab density functional theory calculations, which reveal the relative ordering of adsorption energies for Mn and Bi adsorbed on the different wurtzite facets (Table S2 in the Supporting Information). The highest adsorption energy on the (001) facet (−2.43 eV) indicates that Mn dopants are easily doped into nanowires along the growing axes. Conversely, it is difficult to incorporate the dopants into the lowest adsorption energy surface (110) (−0.45 eV), thus leading to fewer defects and high crystallinity on the (110) facet.

Compared with the undoped nanowires, all reflection peaks of doped nanowires are shifted to the high-angle region and the shift value increases when the Mn content increased from 2.1 to 3.0% (Figure 2d). The increase arises from a reduction in the lattice constant caused by the replacement of large Cd atoms with small Mn atoms.[12] To further confirm Mn doping, energy-filtered TEM (EFTEM) was used to map the nanowires. Figure 3 shows the mapping results of Cd, Se, Mn, and Bi (see area 1 (red rectangle) in Figure S5 in the Supporting Information; this image shows a single wire with a length of 15 μm). It can be seen that traces of Cd and Se are found in the catalyst particle, this result is consistent with the results obtained from energy-dispersive X-ray spectroscopy (EDAX) analysis (Figure S6 in the Supporting Information). The Mn mapping shows that Mn was homogeneously doped into the nanowire. The Bi mapping demonstrates that Bi is mainly at the top end of the nanowire and in fact is found to be entirely absent further along the nanowire (Figure S5 in the Supporting Information). Similar mapping results were obtained from thick short nanowires (Figure S7 in the Supporting Information). The Mn doping can be further proved from the low-temperature (1.7 K) electron paramagnetic resonance (EPR) spectrum (Figure S8 in the Supporting Information), which shows the characteristic six-line hyperfine splitting of Mn^{2+} ($I = 5/2$).[1,3,5] These results confirm that Mn dopants were successfully doped into CdSe nanowires.

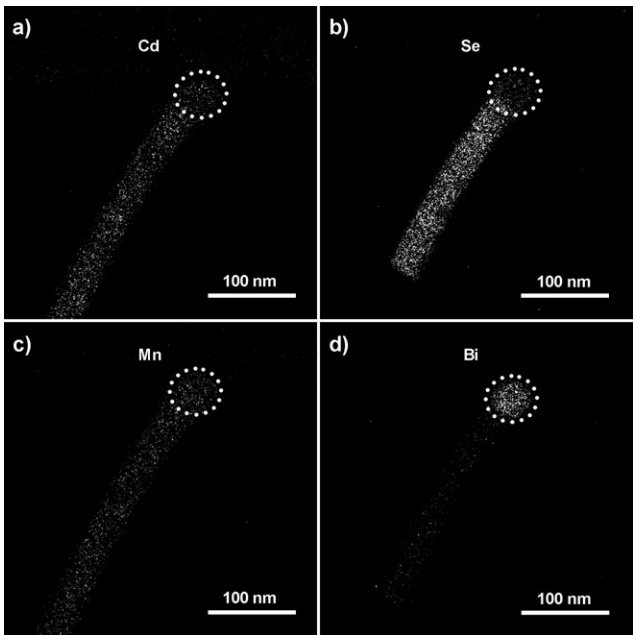

Figure 3. Energy-filtered TEM maps of Cd, Se, Mn, and Bi in the doped nanowire. The nanocatalyst is indicated by the white circle.

The optical properties of doped and undoped nanowires have been characterized with UV/Vis, photoluminescence, and Raman spectroscopy. It can be seen that these nanowires show similar absorption profiles with peaks around 695, 568, and 484 nm (Figure S9a in the Supporting Information). Compared with quantum dots, the nanowire absorption peaks are much broader with lower resolution, which arises from the broader nanowire size distributions. The nanowire absorption features resulted from clusters of closely spaced transitions rather than from individual transitions.[13b] It is known that the valence-band (VB) states are much more closely spaced than the conduction-band (CB) states, because of the greater effective masses of the holes and the hybridized characters caused by mixing heavy-hole and light-hole states.[13b] Therefore, the comparatively large spacing of the CB levels dominates the absorption spectra, such that the first absorption at approximately 695 nm (Figure S9 in the Supporting Information) constitutes a cluster of transitions including $VB_1 \rightarrow CB_1$ and $(VB_2, VB_3) \rightarrow CB_1$, the second absorption peak at approximately 568 nm arises from clustered transitions of $(VB_3, VB_4) \rightarrow (CB_2, CB_3)$, and the third peak at approximately 484 nm arises from the transitions of $(VB_5, VB_6, VB_7, VB_8) \rightarrow (CB_2, CB_3)$.[18]

The doped and undoped nanowires also show a similar emission signals at 720 nm (Figure S9b in the Supporting Information) because of their similar diameters (Figures S2 and S3 in the Supporting Information). It should be noted that both doped and undoped nanowires have low fluorescent quantum yields (< 1%), which are attributed to the admixture of W and ZB phases (leading to a type II structure).[14] Raman spectra reveal no localized vibrational mode, with longitudinal optical phonon modes (LO) at 206 and 413 cm^{-1} (Figure 4a). The absence of a localized vibration supports the conclusion that Mn was homogeneously doped into CdSe lattice.[5] Therefore, Mn doping does not modify the optical properties of the nanowires because the Mn^{2+} ligand-field excited states ($^4T_1$) lie outside the CdSe band gap because of the large size of the nanowires, so that the optical properties are dominated by CdSe itself.[1]

The successful doping of Mn into the host CdSe lattice results in strong carrier–dopant magnetic exchange interactions, as shown by magnetic circular dichroism (MCD) spectroscopy.[1] It should be noted that the MCD spectrum shown in Figure 4b was collected from thinner Mn-CdSe nanowires with a diameter of (10.3 ± 3.1) nm (Figure S10 in the Supporting Information) at 8 K in a magnetic field of 7 Tesla. Thicker nanowires were aggregated when the nanowire solution was frozen during measurements. The absorption spectrum of the nanowires shows broad peaks at

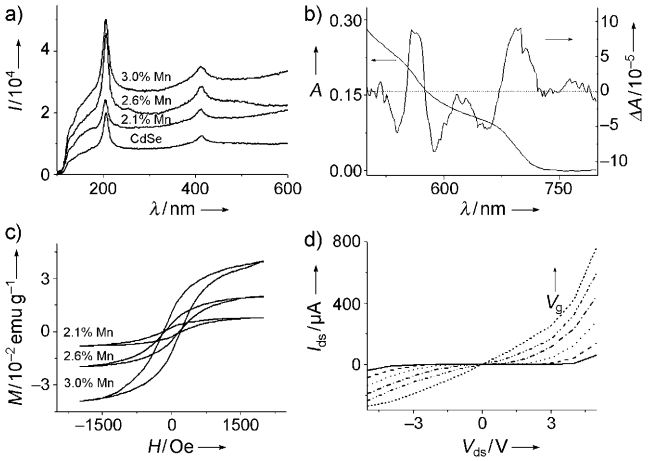

Figure 4. a) Raman spectra of doped CdSe nanowires with different Mn concentrations; b) absorption and MCD spectra of the Mn-doped CdSe nanowires with a diameter of 10 nm measured at 8 K with a magnetic field of 7 Tesla; c) *M*–*H* loops of Mn-doped CdSe nanowires measured at 10 K; d) *I*–*V* curves of field-effect transistors made from Mn-doped CdSe nanowires. $V_g = -20$ V (——), −15 V (– – –), −10 V (••••), 0 V (–•–•), 10 V (–••••), 20 V (-----). ds = source–drain.

approximately 680 and 540 nm, which were attributed to the clustered transitions of $VB_1 \rightarrow CB_1$, $(VB_2, VB_3) \rightarrow CB_1$, and $(VB_3, VB_4) \rightarrow (CB_2, CB_3)$, respectively.[18] In the corresponding MCD spectrum, two positive signals at approximately 696 and 562 nm were detected. It should be noted that no MCD signal was detected at zero field.

Doping of the nanowires with Mn led to low-temperature ferromagnetism (Figure 4c). The saturated magnetizations of these nanowires increased from 7.7×10^{-3} emu g^{-1} to 4.0×10^{-2} emu g^{-1} as the Mn concentration increased. The magnetization temperature dependence was determined by using zero-field cooling (ZFC) and field cooling (FC) procedures in an applied magnetic field of 500 Oe for $10 < T < 300$ K (Figure S11 in the Supporting Information). The ZFC curves show a broad transition temperature around 100 K, which is larger than that of Mn-doped CdSe quantum dots ($D = 4.3$ nm, ca. 50 K).[1a,5a] The broad transition temperature could result from their large size and broad size distribution, which can significantly affect the transition temperature, as demonstrated in magnetic nanoparticles.[19]

The magnetically active CdSe nanowires exhibit good conductivity and they can be used as building blocks for fabricating field-effect transistors (FETs; Figure S12 in the Supporting Information for the FET device structure and the typical SEM image of nanowires between source–drain metal pads). Figure 4d shows the *I*–*V* curves of FET devices fabricated from the Mn-CdSe nanowires shown in Figure 1a. It can be seen that the device shows a pronounced gating effect and the typical behavior of an n-channel FET when the gate voltage was varied from −20 V to 20 V. The n-type conductivity most likely results from the selenium vacancies in the nanowires.[20] In addition, the I_{ds} values in the positive region are higher than the corresponding values in the negative region. This asymmetry indicates the local electron accumulation at the interface induced by the positive bias.[20]

In summary, a novel SLS approach has been developed to prepare diluted magnetic semiconductor nanowires, using manganese-doped cadmium selenide as an example. The doping process is confined within the Bi nanocatalysts and Mn dopants are homogenously doped into the nanowires. The introduction of Mn does not alter the optical properties of the nanowires as the dopant ligand field excited states lie outside the band gap of nanowires, but leads to ferromagnetism and good conductivity of these nanowires, which have great potential applications for fabrication of various photonic, electronic, and magnetic nanodevices.

Experimental Section

Materials: Cadmium oxide (CdO, 99.99%), selenium powder (Se, 99%), octanoic acid (OCA, 99%), octyl ether (99%), and phenyl ether (99%) were purchased from Aldrich. Trioctylphosphine oxide (TOPO, 98%) and trioctylphosphine (TOP, 90%) were purchased from Merck and Fluka, respectively. Bi nanoparticles were prepared according to previously reported methods.[15] The preparation of manganese stearate ($MnSt_2$) is described in the Supporting Information. Other solvents and chemicals were used as received.

Preparation of nanowires: Mn-doped and undoped CdSe nanowires were prepared by a typical solution–liquid–solid (SLS) process where bismuth (Bi) nanoparticles were used as catalysts.[13–15] A mixture of CdO, TOPO, and OCA were loaded into a 50 mL three-necked flask. This mixture was dried and degassed for 30 min at 130 °C under vacuum. Then the flask was back-filled with N_2 and the temperature was increased to 300 °C, which resulted in a clear solution, and the temperature was then reduced to 250 °C. In a separate flask, $MnSt_2$ (250 mg) was dissolved in phenyl ether (10 mL) in presence of OCA (0.5 mL) at 100 °C under the protection of N_2. A mixture of the Mn precursor solution, Bi nanoparticles, and TOPSe was quickly injected into the Cd precursor solution at 250 °C. The solution turned brown within seconds and was kept at 250 °C for 1 min before cooling. When the temperature was reduced to 80 °C, 2–4 mL of toluene was added to the solution to prevent the TOPO from solidifying. The resultant nanowires were separated from solution by high-speed centrifugation (14800 rpm, 10 min) and washed several times with toluene. The purified nanowires can be well redispersed in chloroform and 2-methyltetrahydrofuran (2-MTHF). A summary of reaction parameters and reagent quantities are given in Table S1 in the Supporting Information.

Fabrication of field-effect transistors (FETs): The Mn-CdSe nanowires were spin-coated onto a SiO_2 (300 nm)/Si (p+) substrate. Layers of Cr (4 nm) and Au (100 nm) were subsequently deposited to construct the source and drain electrode employing a shadow mask with a channel length of 35 μm and 40 mm channel width. The gate electrode was formed on the reverse side of the Si substrate by sequential deposition of 4 nm Cr, followed by 100 nm Au. The conductivity measurements were carried out using a probe station and Agilent semiconductor analyzer B1500A installed in a glove box.

Characterization: Transmission electron microscopy (TEM) images were recorded on a JEOL 1010 operating with an acceleration voltage of 100 kV. High-resolution TEM images and energy-filtered TEM (EFTEM) maps were performed on a FEI Tecnai G2 F30 TEM installed with a Gatan GIF200 system and a CCD camera (MSC 794), operating at an acceleration voltage of 300 kV. Energy-dispersive X-ray spectroscopy (EDS) measurements were collected on a FEI Tecnai G2 F20 TEM operating at an acceleration voltage of 200 kV and equipped with a DX-4 analyzer (EDAX). Scanning electron microscopy (SEM) images were recorded on a JEOL JSM6400F. Powder X-ray diffraction measurements were carried out on a Bruker D8 Advanced Diffractometer at 40 kV and 30 mA using $Cu_{K\alpha 1}$ radiation ($\lambda = 1.54056$ Å). UV/Vis spectra were measured with a Shimadzu UV-

2450 spectrometer. Raman and photoluminescence of nanowires were recorded with a laser Raman spectrometer. EPR spectra were recorded on a Bruker Elexsys E500 CW EPR Spectrometer at 1.7 K. The sample was kept under nitrogen after removal of oxygen. Magnetic properties were measured at 10 K by using a Quantum Design magnetic property measurement system (MPMS). ZFC/FC curves were obtained in an applied magnetic field of 500 Oe. Magnetic circular dichroism (MCD) experiments were performed at 8 K with a magnetic field of 7 Tesla (Oxford Instruments Spectromag). The samples were dissolved in 2-MTHF and then frozen into glasses in 2 mm thick quartz cells. The Mn concentration in the nanowires was determined by inductively coupled plasma mass spectrometer (ICP-MS) after digestion in nitric acid.

Theoretical calculations: Geometrical structures were optimized with the Vienna ab initio simulation package (VASP)[21] for implementation of the density functional theory. The generalized gradient approximation (GGA)[22] used for the calculations was the spin-polarized Perdew–Wang 1991 (PW91) formulation.[22] The interaction between ions and electrons was described using ultrasoft pseudopotentials (US-PP) supplied by VASP. Surfaces were represented by six-layer slabs with the theoretical equilibrium lattice constant, and a $6\times6\times1$ k-points grid was used. For the spin-polarized adsorbate calculations, 2×2 supercells were used to represent isolated Mn/Bi adsorbates; within this cell, full relaxation was performed for the top three layers while the bottom three layers were fixed. Gas-phase Mn and Bi atoms were simulated in a box 10 Å on a side, large enough to ensure negligible interactions between neighboring cells. The adsorption energy (E_{ad}) was calculated according to the expression: $E_{ad}=E_{(slab+Mn/Bi)}-(E_{slab}+E_{Mn/Bi})$.

Received: December 14, 2009
Published online: March 5, 2010

Keywords: doping · field-effect transistors · magnetic properties · manganese · nanostructures

[1] a) R. Beaulac, L. Schneider, P. I. Archer, G. Bacher, D. R. Gamelin, *Science* **2009**, *325*, 973 – 976; b) S. T. Ochsenbein, Y. Feng, K. M. Whitaker, E. Badaeva, W. K. Liu, X. Li, D. R. Gamelin, *Nat. Nanotechnol.* **2009**, *4*, 681 – 687; c) R. Beaulac, P. I. Archer, S. T. Ochsenbein, D. R. Gamelin, *Adv. Funct. Mater.* **2008**, *18*, 3873 – 3891; d) J. D. Bryan, D. R. Gamelin, *Prog. Inorg. Chem.* **2005**, *54*, 47 – 126.

[2] a) D. J. Norris, A. L. Efros, S. C. Erwin, *Science* **2008**, *319*, 1776 – 1779; b) S. C. Erwin, L. J. Zu, M. I. Haftel, A. L. Efros, T. A. Kennedy, D. J. Norris, *Nature* **2005**, *436*, 91 – 94.

[3] F. V. Mikulec, M. Kuno, M. Bennati, D. A. Hall, R. G. Griffin, M. G. Bawendi, *J. Am. Chem. Soc.* **2000**, *122*, 2532 – 2540.

[4] N. Pradhan, D. Goorskey, J. Thessing, X. G. Peng, *J. Am. Chem. Soc.* **2005**, *127*, 17586 – 17587.

[5] a) D. Magana, S. C. Perera, A. G. Harter, N. S. Dalal, G. F. Strouse, *J. Am. Chem. Soc.* **2006**, *128*, 2931 – 2939; b) K. M. Hanif, R. W. Meulenberg, G. F. Strouse, *J. Am. Chem. Soc.* **2002**, *124*, 11495 – 11502.

[6] Y. A. Yang, O. Chen, A. Angerhofer, Y. C. Cao, *J. Am. Chem. Soc.* **2008**, *130*, 15649 – 15661.

[7] D. A. Bussian, S. A. Crooker, M. Yin, M. Brynda, A. L. Efros, V. I. Klimov, *Nat. Mater.* **2009**, *8*, 35 – 40.

[8] P. T. K. Chin, J. W. Stouwdam, R. A. J. Janssen, *Nano Lett.* **2009**, *9*, 745 – 750.

[9] J. H. Yu, X. Liu, K. E. Kweon, J. Joo, J. Park, K.-T. Ko, D. Lee, S. Shen, K. Tivakornsasithorn, J. S. Son, J.-H. Park, Y.-W. Kim, G. S. Hwang, M. Dobrowolska, J. K. Furdyna, T. Hyeon, *Nat. Mater.* **2010**, *9*, 47 – 53.

[10] J. S. Kulkarni, O. Kazakova, J. D. Holmes, *Appl. Phys. A* **2006**, *85*, 277 – 286.

[11] B. D. Yuhas, D. O. Zitoun, P. J. Pauzauskie, R. R. He, P. D. Yang, *Angew. Chem.* **2006**, *118*, 434 – 437; *Angew. Chem. Int. Ed.* **2006**, *45*, 420 – 423.

[12] C. C. Chen, Y. J. Hsu, Y. F. Lin, S. Y. Lu, *J. Phys. Chem. C* **2008**, *112*, 17964 – 17968.

[13] a) F. D. Wang, A. G. Dong, J. W. Sun, R. Tang, H. Yu, W. E. Buhro, *Inorg. Chem.* **2006**, *45*, 7511 – 7521; b) J. Sun, W. E. Buhro, L.-W. Wang, J. Schrier, *Nano Lett.* **2008**, *8*, 2913 – 2919.

[14] M. Kuno, *Phys. Chem. Chem. Phys.* **2008**, *10*, 620 – 639.

[15] a) Z. Li, A. Kornowski, A. Myalitsin, A. Mews, *Small* **2008**, *4*, 1698 – 1702; b) Z. Li, Ö. Kurtulus, F. Nan, A. Myalitsin, Z. Wang, A. Kornowski, U. Pietsch, A. Mews, *Adv. Funct. Mater.* **2009**, *19*, 3650 – 3661; c) Ö. Kurtulus, Z. Li, A. Mews, U. Pietsch, *Phys. Status Solidi A* **2009**, *206*, 1752 – 1756; d) N. Fu, Z. Li, A. Myalitsin, M. Scolari, R. T. Weitz, M. Burghard, A. Mews, *Small* **2010**, *6*, 376 – 380.

[16] G. M. Dalpian, J. R. Chelikowsky, *Phys. Rev. Lett.* **2006**, *96*, 226802.

[17] P. Villars, A. Prince, H. Okamoto, *Handbook of Ternary Alloy Phase Diagrams*, *Vol. 5*, ASM International, **1995**.

[18] J. Li, L. W. Wang, *Nano Lett.* **2003**, *3*, 101 – 105.

[19] Z. Li, B. Tan, M. Allix, A. I. Cooper, M. J. Rosseinsky, *Small* **2008**, *4*, 231 – 239.

[20] C. Liu, P. Wu, T. Sun, L. Dai, Y. Ye, R. Ma, G. Qin, *J. Phys. Chem. C* **2009**, *113*, 14478 – 14481.

[21] G. Kresse, J. Hafner, *Phys. Rev. B* **1993**, *47*, 558 – 561.

[22] J. P. Perdew, Y. Wang, *Phys. Rev. B* **1992**, *45*, 13244 – 13249.

